Numerical analysis of multi-loop thermal management

Chi Kit. Cheung*
Department of Aeronautical and Automotive Engineering,
Loughborough University, Leicestershire LE11 3TU, UK

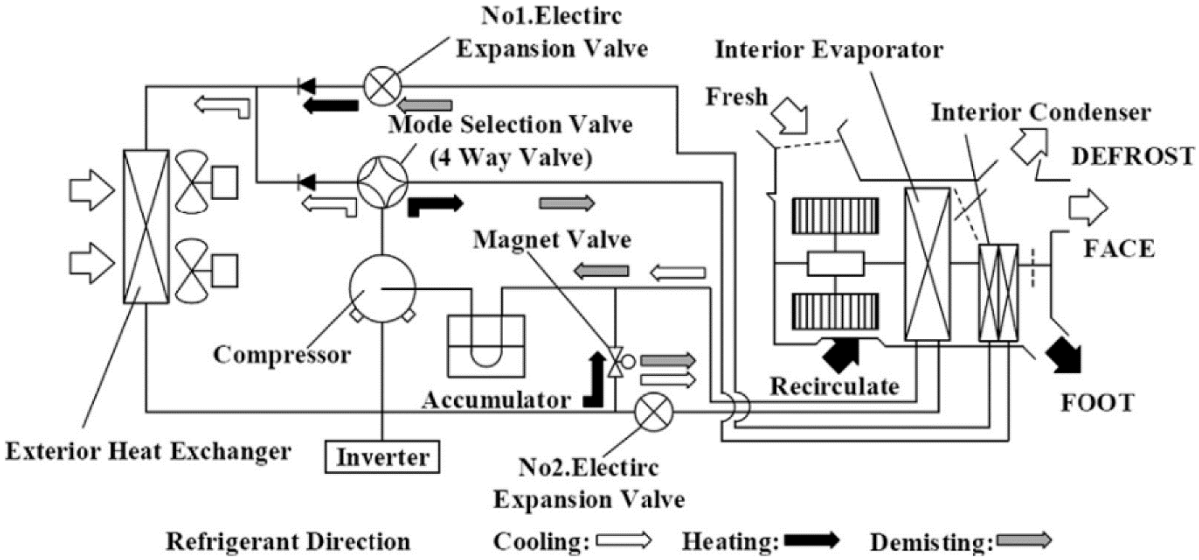

In recent years, the Electric vehicle (EV) including Battery Electric vehicle (BEV) or Fuel Cell Electric Vehicle (FCEV) has attracted more attention in the automotive industries due to the increasing concern and awareness of global warming. In addition, one of the biggest challenges that all the EVs are facing is the relatively low driving range compared to conventional internal combustion engine (ICE) vehicle due to the energy density of the battery. Although battery development has been a major mission in the EV industries, some research had presented that the heating, ventilation, air-condition (HVAC) system have a significant impact on the driving range when it is operating. So it is also important to develop a more efficient system to improve the driving range of the EV. Moreover, the potential of heat pump (HP) system in HVAC has attracted more attention in the EV industries due to better efficiency. Therefore, in this project, the HVAC system based on vapour compression refrigeration (VCR) and HP has been modelled and analysed theoretically. Nevertheless, the environmental impact from the refrigerants also been discussed and the enhancement of the HVAC using an internal heat exchanger with the alternative refrigerant had also been investigated.

* Automotive Engineering MEng; B727149; Project supervisor: Prof F. Rui Chen

1. Introduction

In any automobile design, the thermal management system (TMS) is one of the fundamental functions systems, as it is in charge of maintaining optimal working temperatures to prevents any failures due to overheating. In addition, HVAC system in TMS is also important as the driving performance can be affected by the cabin environment for the driver [1]. For the convection-al EV, the air conditioning (AC) system configuration is rather similar in comparison to a most ICE vehicle. When it comes to cabin cooling, the vapour-compression cycle (VCC) is commonly used has always been the go-to approach in the automotive industries.

On the other hand, for cabin heating, ICE vehicles can utilize the waste heat from the ICE or exhaust gas to provide cabin heating, even when the vehicle is idling. However, the EVs do not produce enough waste heat when idling in order to utilise this method and must use will require other methods such as the use of a positive temperature coefficient (PTC) heater to provide heating for the cabin or air source heat pump (HP) which can be more efficient at a lower temperature compared to PTC [2].

Although the use of an AC is very convenient and can provide a comfortable environment in the cabin, the energy consumption of the system is significant and must also need to be considered. It is because an inefficient AC system can directly affect the performance of a vehicle in terms of driving range which is one of the biggest problems that the current modern EVs are facing. Moreover, a typical AC system can cause about 30 to 40% driving range reduction on EV depending on the size of the AC system and the drive cycle [3][4]. Therefore, the development in AC systems is very important in order to extend the driving range performance of the EV,

However, since the VCC in the AC system uses refrigerant as a heat transfer medium, the environmental impact of the refrigerant being chosen and used also needs to be considered and contemplated. In fact, due to the ozone damage caused by the formerly used hydrochlorofluorocarbons (HCFCs) type of refrigerants such as R123 or R124. The hydrochlorofluorocarbons (HCFCs) type of refrigerant were gradually phased out and replaced with hydrofluorocarbons (HFCs) in accordance to the Montreal Protocol agreement, which was made and imposed in 1987 [5].

For the global warming concern, the HFCs are required to be phased out by 2019 under the amendment to Montreal Protocol. Therefore, one of the most common refrigerants R134a was required to be replaced in automobile AC, due to its global warming potential (GWP) of 1430. In addition, the new hydrofluoroolefin (HFO) refrigerant R1234yf presents as a desirable choice for a replacement, as it has only 4 GWP with 0 ozone depletion potential (ODP). Moreover, the R1234yf was designed to have comparable thermodynamic properties to R134a, hence minimal alterations are required from the current AC system in order to adopt this new refrigerant. [6].

The natural refrigerants such as R729 (Air), R744 (Carbon dioxide CO2) and R717 (Ammonia NH3) seems to have more promising potential for long-term operation. Since the R744 has only 1 GWP and R717 has less than 1 GWP while R729 has 0 GWP and ODP [7]. However, despite the advantage of environmental friendliness, there are some limitations with these natural refrigerants due to their physical properties. For example, the R744

requires a high operating pressure as it has a low critical temperature (-31°C) which leads to higher leak potential [8], the R717 is poisonous in high concentration and is not compatible with copper [9] and R729 needs high mass flow rate in the system due to low specific heat capacity, which leads to large and more complex system design [10]. Table 1 summarises the characteristic of the all the refrigerants that have been discussed.

Table 1 Refrigerant Characteristics

Refrigerant	Classification	GWP	Limitation
R134a	HFC	1430	High GWP
R1234yf	HFO	4	low flammability
R729 (Air)	Natural refrigerant	0	Complex design & high running cost
R744 (CO2)	Natural refrigerant	1	High operation pressure
R717 (NH3)	Natural refrigerant	<1	Toxicity, not compatible with copper

By considering all the advantage and disadvantages of all the available refrigerants, the R1234yf is still considered as the most feasible and suitable replacement of R134a for the EV application due to similar thermodynamic properties and current technological restraints. In this project, the objectives are analysing the R1234yf performance by comparing with R134a on a proposed HVAC models at different environment temperatures and investigating the effects of internal heat exchanger and its potential enhancement of the performance of the HVAC system.

2. Background

2.1. Pressure-Enthalpy diagram for R134a and R1234yf [11]

The figure 1 below shows the thermal properties of the R134a and R1234yf against each other. In the figure 1, the line where the blue arrow is pointing represents the saturated liquid (SL) line of the refrigerant, so when the refrigerant properties is at any point outside the SL line, the refrigerant will become subcooled liquids.

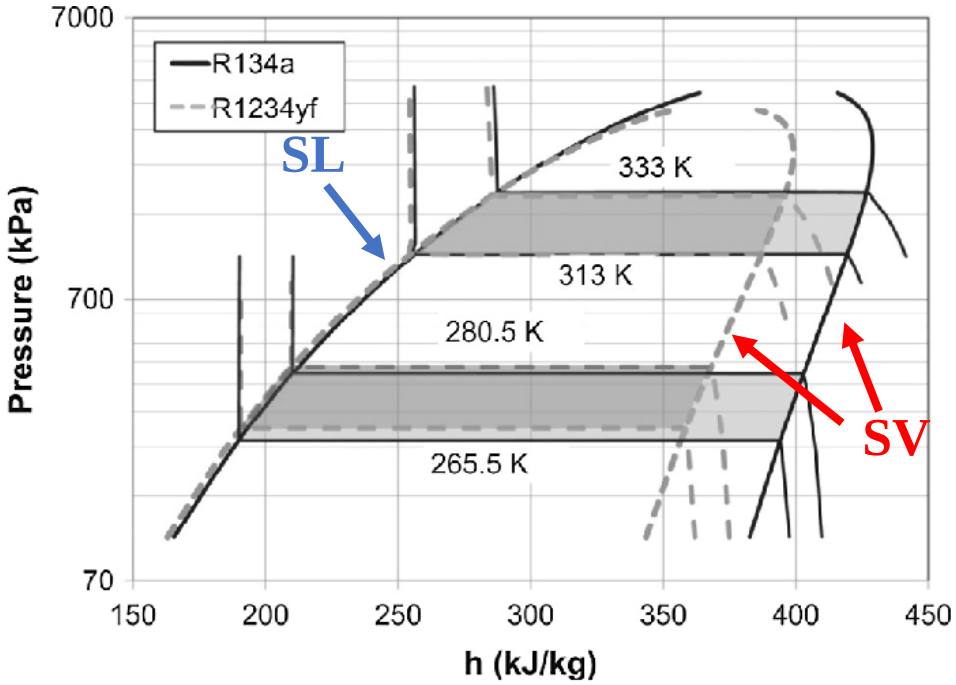

Fig. 1 R134a & R1234yf thermal properties on Pressure-Enthalpy diagram

On the other hand, the line where the red arrow is pointing is the saturated vapour line, so the refrigerant will become a superheated vapour when its properties is at any point is outside the SV line. In addition, the region in between the SV and SL line is the liquid-vapour mixture region and the percentage of the liquid / vapour can be rated from 100% liquid on the SL line to 100% vapour on the SV line. Nevertheless, the straight horizontal line with temperature is the isotherm line. As long as the thermal properties are on this line, the temperature of the refrigerant remains constant.

By observing figure 1, it can be seen that the SL line for R134a and R1234yf are almost identical. However, it also shows that the SV line for R134a is much further right in the graph compared to the SV line for R1234yf. This indicate that for R134a, the amount of enthalpy that is required to become saturated vapour from saturated liquid or vice versa is greater than R1234yf, therefore the R134a can absorb or reject more energy at a constant pressure and temperature. Thus theoretically, the R134a will have a better performance than the R1234yf.

2.2. Vapour Compression Cycle (VCC)

The vapour compression cycle is based on the concept of reversed Carnot Cycle and it consists 4 main components, a compressor, condenser, evaporator, and expansion valve, which is arranged in the order shown in figure 2.

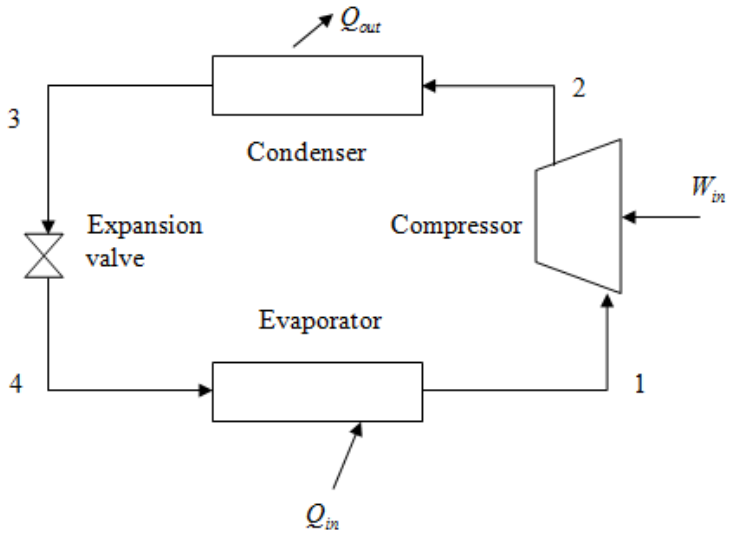

Fig. 2 Schematic of Vapour Compression Cycle

For better understanding of the VCC in terms of thermodynamics, the figure 2 below presents the ideal VVC on a temperature-entropy and pressure-enthalpy diagrams on the left and right respectively.

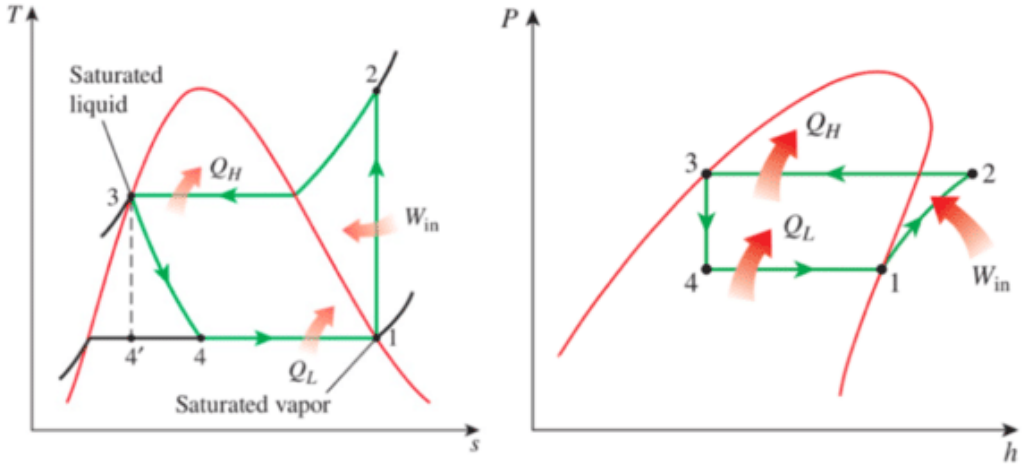

Fig. 3 Temperature-Entropy diagram (left) and Pressure-Enthalpy diagram (right)

For the thermodynamic stage 1 to 2, isentropic compression takes place and the pressure and temperature of the refrigerant increase while no heat is exchanged with the environment, hence the enthalpy of the cycle increase, and entropy remain constant.

Then, from stage 2 to 3, the superheated, high pressure and temperature refrigerant vapour will enter the condenser and will be cooled at a constant pressure (isobar process) until it reaches its saturated vapour point. After that, the refrigerant will change phase from vapour into a liquid-vapour mixture at a constant temperature (isotherm process) until it reaches its saturated liquid point. The heat from the cycle is rejected during this process, causing both entropy and enthalpy of the system decreases.

After that, from stage 3 to 4, the refrigerant will enter the expansion valve and will change its phase from saturated liquid into liquid-vapour mixture. During this phase change, while

the temperature and pressure decreases, the whole process is considered as isenthalpic, and no work is done and no heat is exchanged on or by the environment, so the enthalpy remains constant, but the entropy increases.

Finally, from stage 4 to 1, the refrigerant will enter the evaporator, absorbing the heat from the environment whilst maintaining its temperature and pressure, hence the process is isotherm and isobar, and the entropy and enthalpy of the system increases. The refrigerant will then change its phase from liquid-vapour mixture to saturated vapour before it enters the compressor again for the next cycle.

2.3. Coefficient of Performance

For the coefficient of performance (COP) of the cycle or system, it can be defined and shown in Eq.1.

$$COP \text{ of the cycle/system } == \frac{Cooling\ effect\ /\ Heating\ effect}{Total\ work\ input\ in\ to\ cycle/system} \quad (1)$$

2.4. VCC Enhancement with integrated internal heat exchanger

According to Pottker and Hrnjak (2014) [12], the potential COP improvement can be achieved by subcooling the liquid before the isenthalpic expansion device, as it can reduces the throttling losses. As shown in the figure 4, this can be achieved with the use of an internal heat exchanger, which sub-cools the refrigerant before it enters the expansion valve. This leads to a reduction in the vapour quality at the evaporator inlet, resulting in an increase in refrigerating effect (shown in figure 5, h6-h5 > h6-h5'). However, due to the heat transfer between refrigerant, the refrigerant is superheated further which results in a higher specific volume at the inlet of the compressor, hence more work is required to compensate for the decrease in mass flow rate [13].

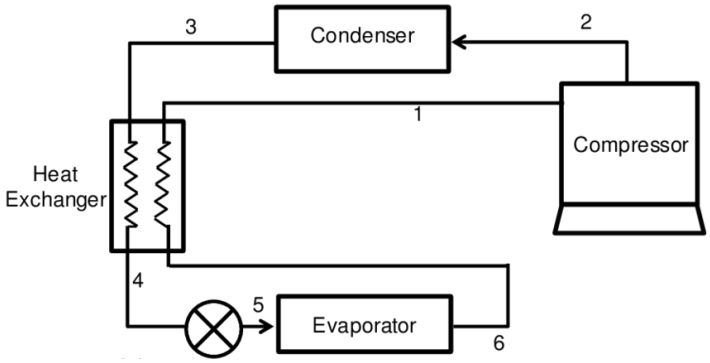

Fig. 4 Schematic of VVC with IHX

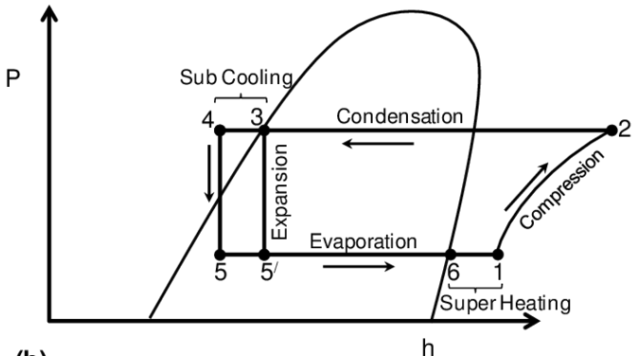

Fig. 5 VVC with IHX on Pressure-Enthalpy diagram

3. Technical Achievement

In this section of the project, the technical achievement including modelling and simulation results will be discussed. In order to understand the modelling of the HVAC system in Simulink with Simscape package, it is very important to be familiar with the mathematic expression of each component's model which will be studied and explained in later section. In order to investigate the effect of internal heat exchanger in both vapour compression refrigeration and heat pump cycle of the HVAC system, the proposed HVAC system were separated, and 2 individual models were made for the cooling mode and heating mode as this can reduce the calculation load and complying time of the model in Simulink, therefore, 4 four models in total were developed.

Two of the models are reference models which will be used to demonstrate the behaviour of the HVAC system in cooling and heating mode, and the other two models will be similar but with the addition of an internal heat exchanger. By comparing the models against each other, the effects of the internal heat exchanger on the cooling and heating mode can be investigated, respectively. After that, the reference models will run 2 sets of simulations, one with refrigerant R134a, and one with refrigerant R1234yf. These results will be expected to show that refrigerant R134a has a much higher performance than refrigerant R1234yf. However, the two models with the internal heat exchanger (IHX) will then run a simulation using R1234yf. These results will be used to investigate and analyse the COP enhancement with IHX and using R1234yf.

3.1. Proposed HVAC System Overview

As it is shown in the Fig. , the proposed HVAC system contains several key components and are listed below:

- Outdoor heat exchanger (OHX) which can be act as an evaporator or condenser depending on what mode it is currently on.
- Cabin condenser (CON) for heating mode
- Cabin evaporator (EVA) for cooling mode
- Expansion valve (EXV) for controlling the refrigerant flowrate.
- Compressor (COMP)
- 3-way valves (3V) which is used to control the refrigerant flow direction
- Fan (FAN) and blower (B) which are used to provide air flow though the OHX and cabin.

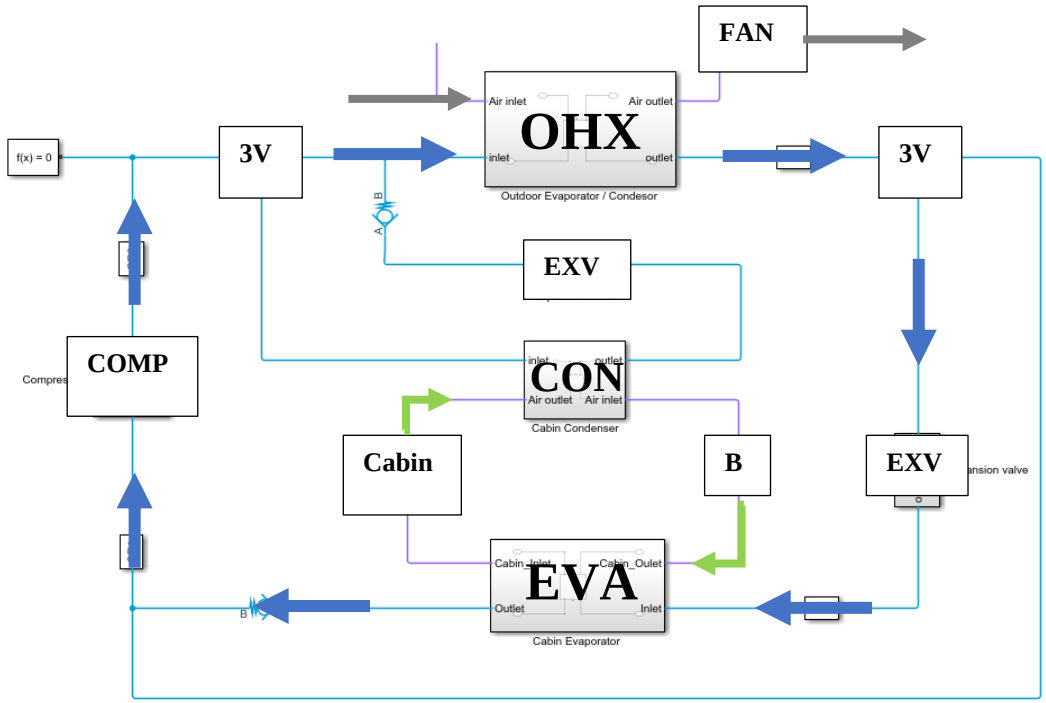

Fig. 6 Schematic of the HVAC system model in Cooling mode

The blue arrow in the figure 6 indicates the refrigerant flow when the system is in cooling mode. the grey arrow and green arrow represent the outdoor air flow and indoor air flow direction, respectively. Note that the OHX is used as a condenser and rejects heat to the outside environment. In addition, the figure 7 shows the schematic of the proposed HVAC system with heating mode, note that the red arrow in the figure 7 indicate the refrigerant flow in heating mode.

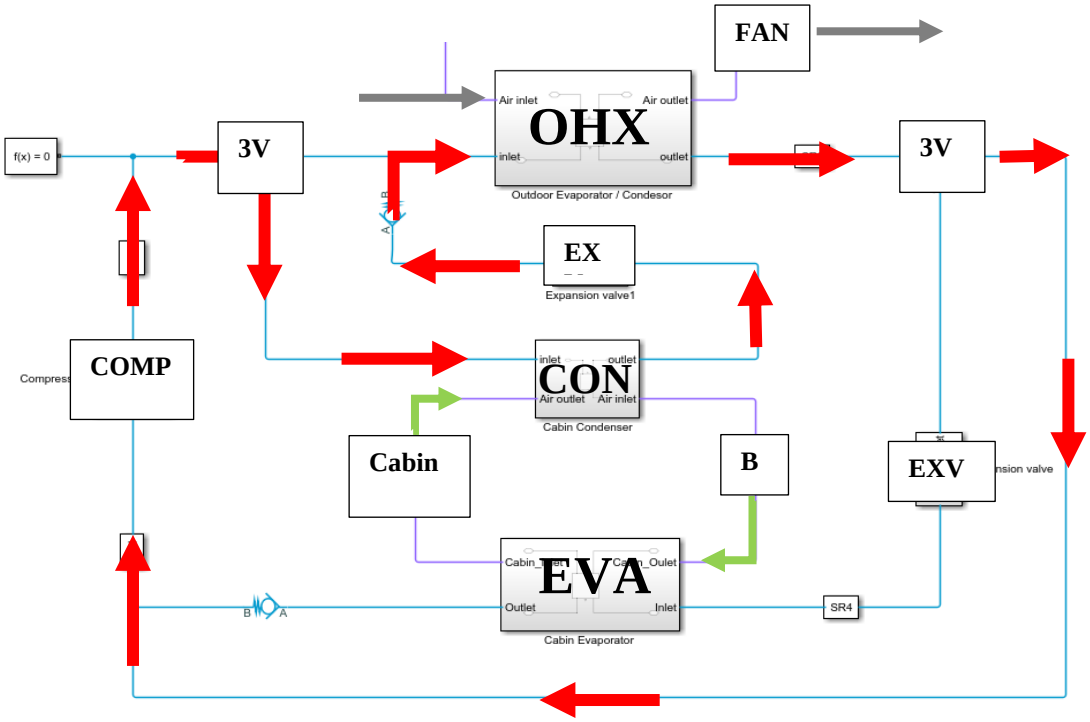

Fig. 7 Schematic of the HVAC system model in Heating mode

3.2. Cooling and Heating Model

The figure 8 and 9 below show the reference model when the system is in cooling and heating mode, respectively. Note that the number in a circle indicates the value at different cycle point, for example, the enthalpy at cycle point 1 will be equal to h_1.

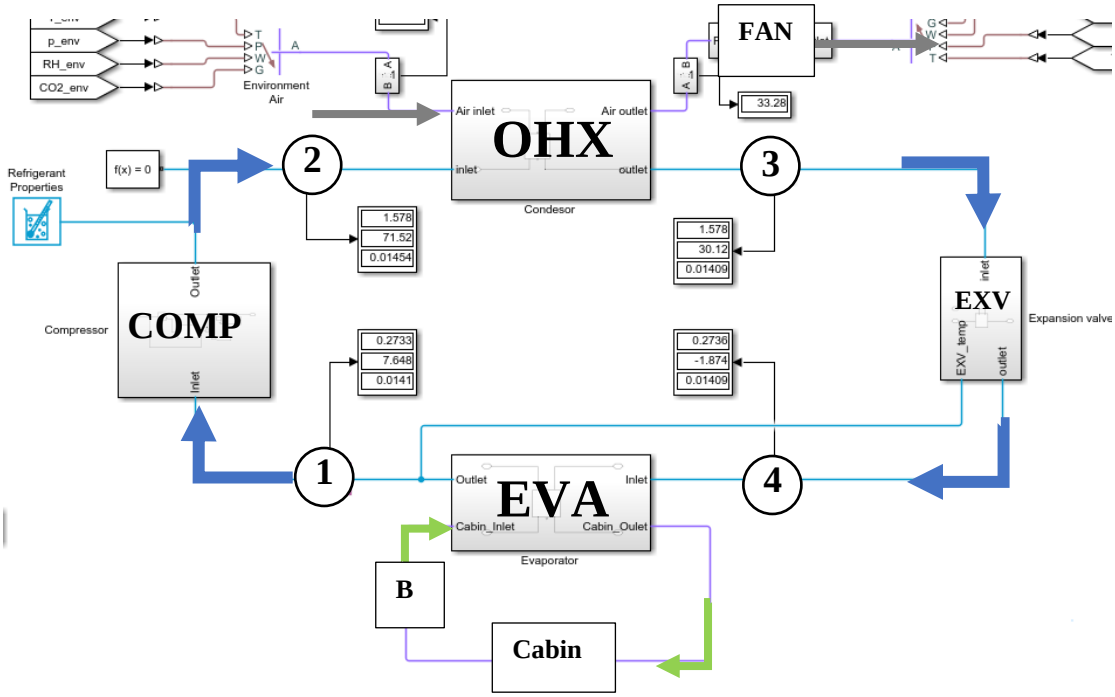

Fig. 8 Cooling mode model

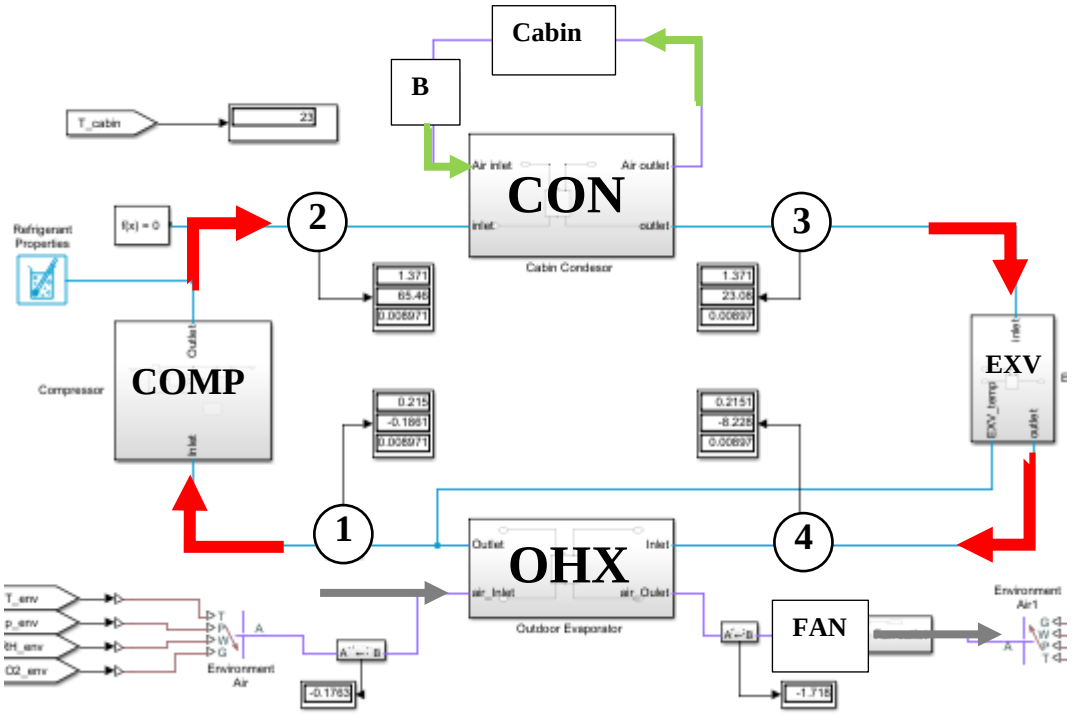

Fig. 9 Heating mode model

3.3. Cooling and Heating Model with IHX

The figure 10 and 11 shows the schematic of the cooling and heat model with integrated internal heat exchanger.

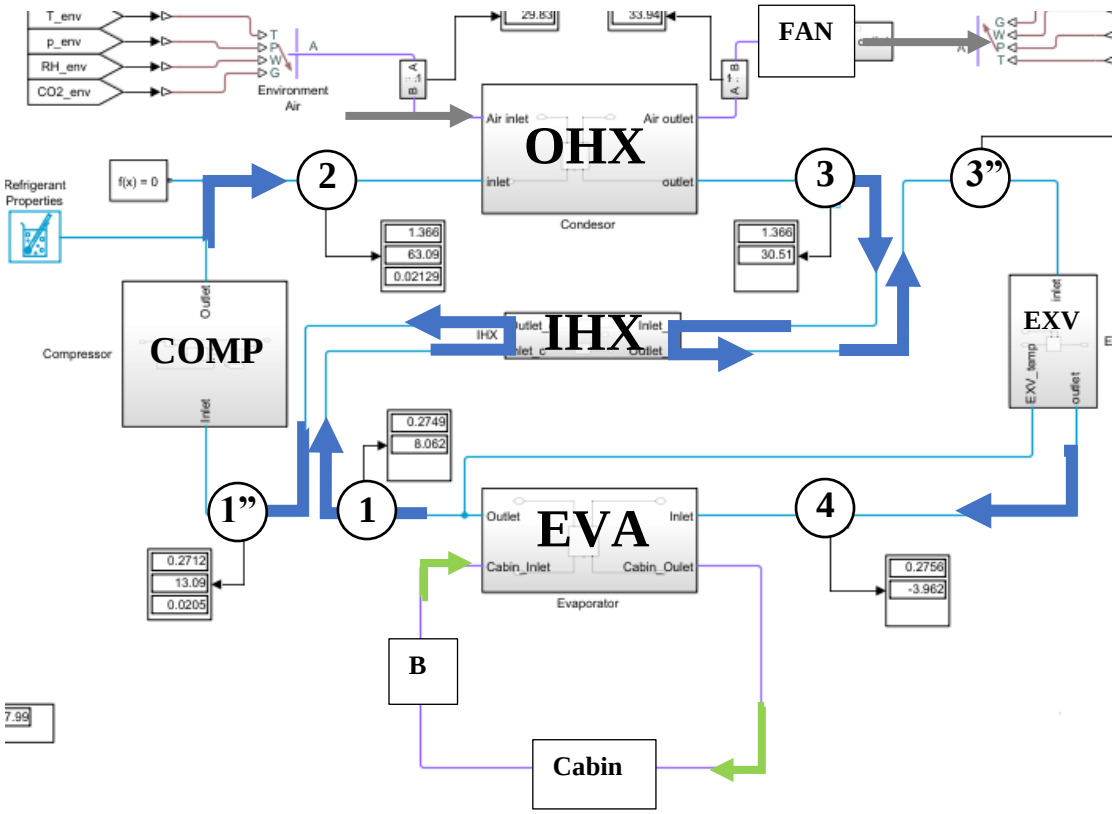

Fig. 10 Cooling mode model with IHX

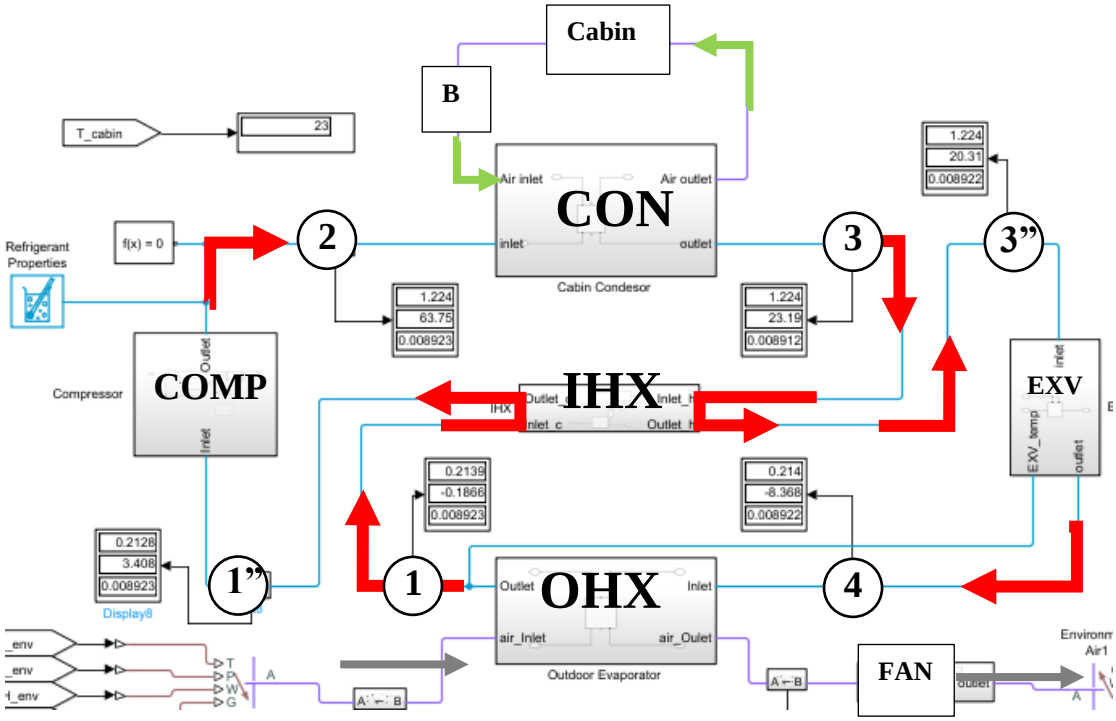

Fig. 11 Heating mode model with IHX.

3.4. Compressor Model

For the compressor model, it is assumed as isentropic reciprocating compressor, which means no heat transfer between the compressor and the environment and the process is reversible, the isentropic suction volumetric flow rate $\dot{V}_{s-s}$ can be determined in Eq. (2).

$$\dot{V}_{s-s} = \eta_{cl} \cdot N \cdot V_{disp} \tag{2}$$

Where N is the compressor rotational speed, V_{disp} is the compressor displacement or suction stroke swept volume and η_{cl} is the clearance volumetric efficiency for an isentropic compressor[14]. However, in reality, the actual volume flow rate will always be less than the isentropic volumetric flow rate due to different factors, for example, the pressure drop between the suction and discharge valve, the heat transfer between the refrigerant and the compressor wall and the pressure ratio between suction and discharge [15]. Therefore, to estimate the actual suction volume flow rate $\dot{V}_s$, the isentropic volume efficiency η_{v-s} is defined in Eq. (3):

$$\eta_{v-s} = \frac{\dot{V}_s}{\dot{V}_{s-s}} \tag{3}$$

where v_s is the specific volume of the suction refrigerant. However, in order to get a more realistic performance of the compressor, according to research that have been done by Adrián Mota-Babiloni, Joaquín Navarro-Esbrí, Ángel Barragán, Francisco Molés, Bernardo Peris [16], the volumetric efficiency η_v versus compression ratio (P_c/P_e) data from a was used for the compressor model in this simulation. The figure 12 shows that the volumetric efficiency η_v with R134a and R1234yf at different pressure ratio. Note that the overall η_v for R134a is higher than R1234yf at different pressure ratio.

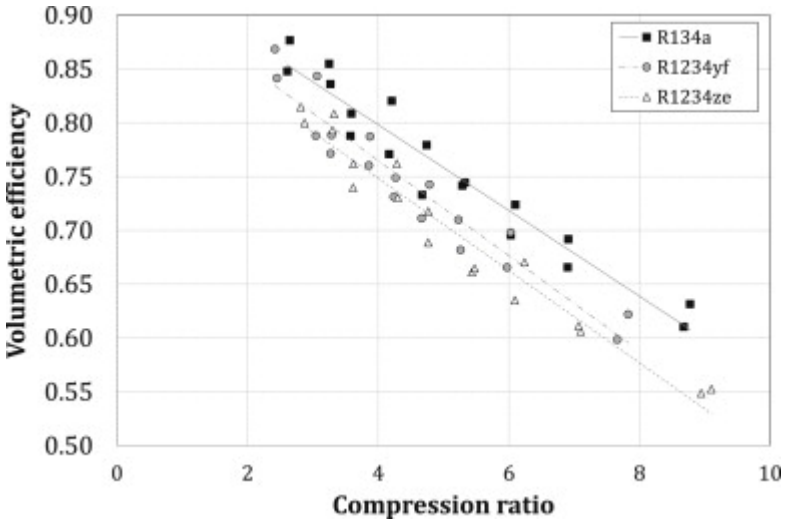

Fig. 6 Compression ratio vs Volumetric efficiency [16]

Therefore, the mass flow rate of the refrigerant can be calculated in the Eq. (4).

$$\dot{m} = \frac{\eta_v \cdot V_{disp} \cdot N}{v_s} \tag{4}$$

To account the effect of the ambient temperature and pressure, the corrected mass flow rate $\dot{m}_c$ is determined in Eq. (5).

$$\dot{m}_c = \dot{m} \cdot \frac{P_s/P_{ref}}{\sqrt{T_s/T_{ref}}} \quad (5)$$

Where the P_{ref} and T_{ref} is the reference Pressure and temperature at a sea level on standard day, the value for P_{ref} = 101.325 kPa and T_{ref} = 288.15 K [17]. To calculate the specific work that is required for isentropic compression w_{c-s}, it can be express as the Eq. (6).

$$w_{c-s} = h_{d-s} - h_s \quad (6)$$

Where h_s is the refrigerant specific enthalpy at suction and h_{d-s} is the discharge refrigerant enthalpy at constant entropy. Once the specific work is known, the power consumption of compressor model $\dot{W}$ can be determined in the Eq. (7).

$$\dot{W} = \dot{m}_c \cdot (h_{d-s} - h_s) \quad (7)$$

3.5. Outdoor Heat Exchanger, Condenser and Evaporator model

For the simulation purpose, the pressure loss in both condenser and evaporator and OHE due to viscous friction is assumed to be negligible, the general geometries of all the heat exchangers for the simulation are shown in Table 2, 3 and 4.

Table 2. Geometry of Outdoor Heat Exchanger model

Parameters	Value
Overall length (m)	1.2
Overall width (m)	0.015
Overall height (m)	0.39
Number of tubes	40
Tube wall conductivity (W/m/k)	240
Fouling factor on both side of fluids	0.1

Table 3. Geometry of Cabin Evaporator model

Parameters	Value
Overall length (m)	0.63
Overall width (m)	0.015
Overall height (m)	0.2
Number of tubes	20
Tube wall conductivity (W/m/k)	240
Fouling factor on both side of fluids	0.1

Table 4. Geometry of Cabin Condenser model

Parameters	Value
Overall length (m)	0.63
Overall width (m)	0.040
Overall height (m)	0.2
Number of tubes	40
Tube wall conductivity (W/m/k)	240
Fouling factor on both side of fluids	0.1

For both model, it is modelled as fin tube type of heat exchanger. When the refrigerant flows thought these heat exchangers, the phase will change from superheated vapour to liquid/vapour mixture to saturated liquid during condensation and from saturated liquid to vapour during evaporation. So, for the condenser and evaporator model. The total heat transfer rate between the air and the refrigerant through the heat exchanger can be expressed in the Eq. (8)

$$Q = Q_L + Q_M + Q_v \tag{8}$$

Where Q_L, Q_M and Q_v are the heat transfer rate in liquid zone, liquid/vapour mixture zone and vapour zone, respectively. To calculate the heat transfer rate for each zone the $\epsilon - NTU$ method is used, and it can be calculated in Eq. (9)

$$Q_{zone} = \epsilon \cdot C_{min} \cdot \left(T_{r,in} - T_{a,in}\right) \tag{9}$$

Where ϵ is the effectiveness of the condenser or evaporator, C_{min} is the lesser heat capacity of the fluids, $T_{r,in}$ is the refrigerant temperature at the zone inlet in the condenser or evaporator and $T_{a,in}$ is the air temperature zone inlet at the condenser or evaporator.

The ϵ value is determined based on the flow arrangement of the heat exchanger [18]. The fluids flow configuration for the condenser or evaporator model is assumed to be crossflow and unmixed, therefore, ϵ is calculated in Eq. (10).

$$\epsilon = 1 - exp\left\{\frac{NTU^{0.22}}{C_R}\left[exp(-C_R \cdot NTU^{0.78}) - 1\right]\right\} \tag{10}$$

Where C_R is the heat capacity ratio of refrigerants and air and NTU is the number of transfer units, both value can be determined in Eq. (11) and (12).

$$C_R = \frac{C_{min}}{C_{max}} \tag{11}$$

$$NTU = \frac{z}{C_{min} \cdot R} \tag{12}$$

The z in the equation (y) is the length fraction in different zone and R is the total thermal resistance between the refrigerant and air due to convection, conduction and fouling on the tube walls, shown in Eq. (13) below. Each thermal resistance is calculated and shown in Eq. (14) and (15).

$$R = R_{conv} + R_{cond,wall} + R_F \tag{13}$$

On refrigerant side :

$$R_{conv,r} = \frac{1}{U_r \cdot A_r} \tag{14a}$$

$$R_{F,r} = \frac{F_r}{A_r} \tag{14b}$$

On air side :

$$R_{conv,a} = \frac{1}{U_a \cdot A_a} \tag{15a}$$

$$R_{F,a} = \frac{F_a}{A_a} \tag{15b}$$

Where A is the total heat transfer area between the fluids and tube wall and fins. The F represents the fouling factors on both fluids. To calculate the convective heat transfer coefficient U of the fluid, it can be seen in Eq. (16).

$$U = \frac{Nu \cdot k}{D_H} \tag{16}$$

Where k is the fluid phase thermal conductivity and D_H is the hydraulic diameter of the tubes. The Nusselt number Nu_r in the single-phase refrigerant region (subcooled liquid or superheated vapour) is determined with the Gnielinski correlation [19], which is shown in the Eq. (17).

$$Nu_r = \frac{\frac{f_d}{8}(Re - 100)\cdot Pr}{1+12.7\sqrt{\frac{f_d}{8}}(Pr^{2/3}-1)} \quad (18)$$

Where Re and Pr is the Reynolds number and Prandtl number of the fluid, f_d is the Darcy friction factor. For the liquid-vapour mixture zone, the Cavallini-Zecchin correlation was used to calculate the Nusselt number, and the detail description can be found in [19]. In addition, on the air side of both heat exchangers, the Dittus-Boelter correlation [19] was used to calculate the Nusselt number Nu_a and it is shown in Eq. (19).

$$Nu_a = 0.023 \cdot Re^{0.8} \cdot Pr^n \quad (19)$$

The index number $n = 0.4$ when air is being heated through the condenser and $n = 0.3$ as air is being cooled through the evaporator. Finally, to determine the cooling capacity of the evaporator Q_{cool}, the Eq. (20) was used.

$$\dot{Q}_{evap} = \dot{m}_c \cdot (h_{eo} - h_{ei}) \quad (20)$$

Where h_{eo} and h_{ei} is the refrigerant specific enthalpy at the outlet and inlet of the evaporator. In addition, the heating capacity of the condenser Q_{heat} is calculated with Eq.(21) below.

$$\dot{Q}_{cond} = \dot{m}_c \cdot (h_{ci} - h_{co}) \quad (21)$$

Where h_{co} and h_{ci} is the refrigerant specific enthalpy at the outlet and inlet of the condenser.

3.6. Thermal Expansion Valve model

The thermal expansion valve is used to simulate the throttling process in the system. In this model, the process is assumed as isenthalpic so that no heat and work will be done and exchanged between the environment and valve. When it comes to maintaining the minimal level of superheat at the evaporator outlet, the valve takes the pressure and temperature measurement at the evaporator outlet through the bulb to adjust the effective opening area. For example, when the superheat in an evaporator outlet decreases, the valve will close to reduce the flow into the evaporator and result a decrease in heat transfer, thus increasing the evaporator outlet temperature, and vice versa. The Eq. (22) shows the calculation of the effective opening area A_{eff} [20].

$$A_{eff} = \beta \cdot [(P_{bulb} - P_{eq}) - P_{sat} \cdot (T_{evap} + \Delta T_{static}) - P_{sat} \cdot (T_{evap})] \quad (22)$$

Where β is the valve constant determined from the nominal operation conditions, P_{eq} and P_{bulb} is the equalization pressure and the bulb pressure respectively, the P_{sat} represent the saturation pressure of the refrigerant. The T_{evap} and ΔT_{static} represent the nominal evaporating temperature and the static (minimum) evaporator superheat, respectively. For simulation purposes, the T_{evap} is set to 1 °C and ΔT_{static} is set to 5°C.

Therefore, the mass flow rate through the valve is defined and shown in Eq. (23).

$$\dot{m} = A_{eff} \cdot \sqrt{\frac{2}{v_{in}}} \frac{\Delta P}{(\Delta P^2 - \Delta P_{lam}{}^2)^{0.25}} \quad (23)$$

Where v_{in} is the specific volume at the inlet, ΔP is the pressure difference between inlet and outlet of the valve and ΔP_{lam} is the pressure threshold for transitional flow.

3.7. Internal heat exchanger

For the internal heat exchanger, a tube-in-tube type internal heat exchanger (IHX) is modelled, and pressure drop in the IHX is assumed to be negligible due to vicus friction. The schematic of the IHX is shown in figure 13 below. In this model, it is assumed heat transfer only occurs between the hot and cold side of the refrigerant with counter flow configuration.

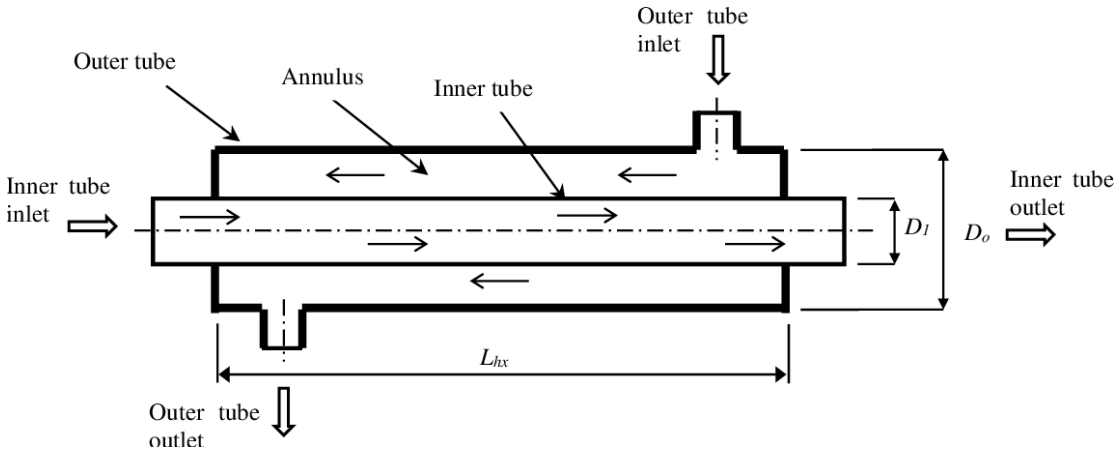

Fig. 13 Schematic of the Internal Heat Exchanger

The thermal resistance due to convection inside the inner and outer tube was calculated using the Eq. (14) and (15) from the section 3.5, however, The heat transfer area A_o for the outer tube is equal to the outer surface area of the inner tube, and A_i is equal to the inner surface area of the inner tube, see figure 14. The general geometry of the IHX model is shown in the table 5 below.

Table 5 Geometry of the IHX model

Parameters	Value
Overall length (m)	0.5
Inner diameter of outer tube (m)	0.02
Inner diameter tube inner tube (m)	0.01
Tube wall thickness (m)	0.001
Tube wall conductivity (W/m/k)	240

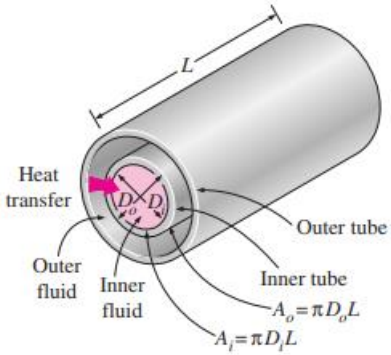

Fig. 14 Heat transfer areas between inner and outer tube [21]

To calculate the thermal resistance R_{wall} due to conduction of the inner tube wall, the Eq. (24) was used to calculate it [21].

$$R_{wall} = \frac{\ln(D_o/D_i)}{2\pi kL} \tag{24}$$

Where D_o and D_i is the diameter of outer and inner tube respectively, k is the thermal conductivity of the tube wall and L is the tube length. By summing up all the thermal resistance due to convection and conduction, the rate of heat transfer can be calculated by

using the $\epsilon - NTU$ method which was described in the section 3.5. The heat transfer rate of the IHX can also be expressed in specific enthalpy term, which shown in Eq. (25).

$$\dot{Q}_{IHX} = \dot{m} \cdot (h_{o,out} - h_{o,in}) = \dot{m} \cdot (h_{i,out} - h_{i,in}) \quad (25)$$

Where $h_{o,out}$ and $h_{o,in}$ is the outer tube specific enthalpy at the outlet and inlet and $h_{i,out}$ and $h_{i,in}$ is the inner tube specific enthalpy at the outlet and inlet.

3.8. Cabin Heat Load Calculation

The thermal load in a typical vehicle can be divided from different source, for example, the solar radiation, the ambient load due to temperature difference between exterior and interior, heat load from passengers and waste heat from the battery or other electronic components etc, see figure 15. In this model, the heat load due to solar radiation, passenger, and ambient were considered.

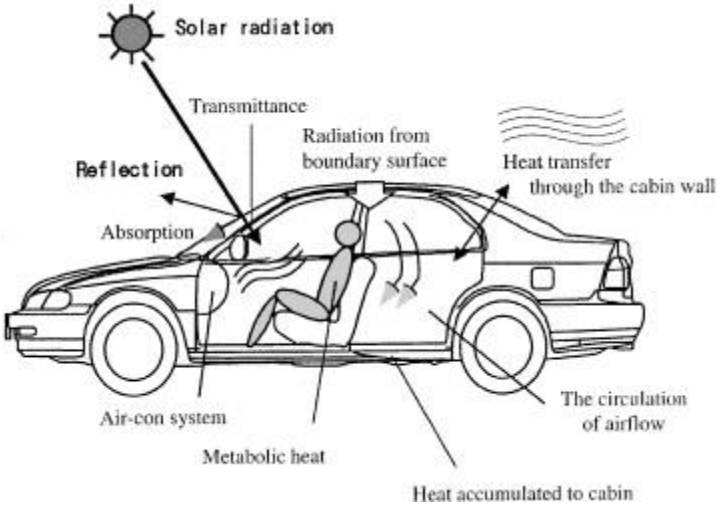

Fig. 15 Thermal load on vehicle cabin

To determine the ambient heat transfer due to conduction and convection, the Eq. (26) and 27 was used.

$$Q_{conduction} = \frac{k_{wall}}{t_{wall}} \cdot A \cdot \Delta T_{wall} \quad (26)$$

$$Q_{convection,in} = h_{in} \cdot A \cdot \Delta T_{in} \quad (27)$$

Where k_{wall} is the thermal conductivity of the cabin wall material, T_{wall} represent the thickness of the wall, ΔT is the temperature difference between the inside, outside of the wall and h_{in} represents the heat transfer coefficient of the air inside the cabin. So, to define the complete ambient heat transfer process, the heat balance Eq.(28) is shown below.

$$h_{out} \cdot \Delta T_{out} = \frac{k_{wall}}{t_{wall}} \cdot \Delta T_{wall} = h_{in} \cdot \Delta T_{in} \quad (28)$$

For the heat load duo to solar radiation, the sol-air temperature concept which is was used and shown in Eq. 29 [22].

$$t_s = t_o + I \cdot \alpha \cdot f_o \quad (29)$$

Where t_s is the sol-air temperature which represents the combined heat transfer effect due to convection and radiation to the surface. t_o is the outside air temperature, I is the total radiation intensity , α is the absorptivity of the surface and f_o outside firm coefficient. So, once the t_s is obtained, the Solar heat can be estimated using the Eq.(30) below.

$$Q_{solar} = U \cdot A_{solar} \cdot (t_s - t_i) \quad (30)$$

Where t_i is the temperature inside the cabin and U is the overall heat transfer coefficient. A_{solar} is the surface area that exposed to the solar radiation. To calculate the total heat load from human body, the Eq.(31) was used.

$$Q_{human} = n \cdot (sensible\ heat\ load + latent\ heat\ load) \quad (31)$$

Where n is the number of occupant.

3.9. Simulation Setting and Data Collection Procedures

For the cooling mode models, it was simulated with different environment temperature range from 30 °C to 40 °C with 2 °C of interval. In addition, the environment temperature was selected from 6 °C to -4 °C with 2 °C interval.

In order to run the simulation, the initial value was set and shown in the Table 6 below for all the models. Note that the air flow of the Fan and Blower were remain constant throughout the entire simulation and all models. The rotation speed of the compression was kept at 1800 rpm.

Table 6 Initial Value for all models

Parameters	Value
Fan air flow (m^3/s)	0.75
Fan constant power (W)	800
Blower flow speed (m^3/s))	0.5
Fan constant power (W)	500
Environment Pressure (Mpa)	0.101325
Initial relative humidity	0.4
EXV min superheat for cooling mode (°C)	5
EXV min superheat for heating mode (°C)	2.5
EXV min subcooling for both mode (°C)	5
Compressor speed (rpm)	1800

For the initial pressure of refrigerant R134a and R1234yf, the value vary according to different initial environment temperature and it is shown in the Table 7 below [23].

Table 7 Initial refrigerant pressures value at different temperature (R134a & R1234yf)

Temperature (°C)	R134a Pressure (Mpa)	R1234yf Pressure (Mpa)
-4	0.15	0.39
-2	0.17	0.42
0	0.19	0.46
2	0.21	0.49
4	0.23	0.53
6	0.26	0.56
30	0.71	1.10
32	0.73	1.20
34	0.75	1.26
36	0.82	1.32
38	0.85	1.39
40	0.9	1.46

For the initial temperature of the cabin, it was assumed to be equal to the outside environment temperature. The data and results was collected when the cabin temperature reached the target temperature, for example, the target temperature for all the cooling mode models is 18 °C and 23 °C for all the heating mode models.

3.10. Results (Cooling mode models)

For the cooling mode simulation, the simulation value from Cooling mode model with the R134a refrigerant is shown in the Table 8 below. In addition, the Table 9 shows the simulation value from the cooling mode model with IHX and R1234yf as the refrigerants.

Table 8 The simulation results from Cooling mode model with R134a and R1234yf

Refrigerant R134a						
Environment Temp (°C)	**30**	**32**	**34**	**36**	**38**	**40**
h_1 (kJ/kg)	406	406	405	405	405	405
h_2 (kJ/kg)	441	442	442	443	444	445
h_3 (kJ/kg)	242	244	247	250	253	255
h_4 (kJ/kg]	242	244	247	250	253	255
P_{cond} (Mpa)	1.33	1.38	1.45	1.52	1.60	1.73
P_{evap} (Mpa)	0.26	0.26	0.26	0.26	0.26	0.26
$\dot{Q}_{cond}$ (W)	2880	2754	2634	2570	2530	2508
$\dot{Q}_{evap}$ (W)	2370	2250	2130	2050	2010	1970
$\dot{W}_{comp}$ (W)	500	503	504	510	521	535
COP_{system}	1.31	1.24	1.18	1.13	1.10	1.07
Refrigerant R1234yf						
Environment Temp (°C)	**30**	**32**	**34**	**36**	**38**	**40**
h_1 (kJ/kg)	371	370	370	370	370	370
h_2 (kJ/kg)	399	400	401	402	403	403
h_3 (kJ/kg)	240	243	245	248	251	254
h_4 (kJ/kg]	240	243	245	248	251	254
P_{cond} (Mpa)	1.39	1.46	1.55	1.64	1.76	1.92
P_{evap} (Mpa)	0.29	0.29	0.28	0.28	0.28	0.28
$\dot{Q}_{cond}$ (W)	2900	2781	2664	2591	2551	2530
$\dot{Q}_{evap}$ (W)	2380	2254	2134	2051	1996	1970
$\dot{W}_{comp}$ (W)	534	535	536	542	556	559
COP_{system}	1.30	1.22	1.16	1.11	1.07	1.04

Table 9 The simulation results from Cooling mode model with IHX using R1234yf

Refrigerant R1234yf with IHX						
Environment Temp (°C)	**30**	**32**	**34**	**36**	**38**	**40**
h_1 (kJ/kg)	371	370	370	370	370	370
$h_{1"}$ (kJ/kg)	376	375	375	375	375	375
h_2 (kJ/kg)	403	404	405	405	406	407
h_3 (kJ/kg)	241	243	246	249	252	255
$h_{3"}$ (kJ/kg)	241	242	243	245	247	249
h_4 (kJ/kg]	241	242	243	245	247	249
P_{cond} (Mpa)	1.21	1.27	1.33	1.41	1.49	1.59
P_{evap} (Mpa)	0.29	0.29	0.29	0.28	0.28	0.28
$\dot{Q}_{cond}$ (W)	2920	2776	2653	2575	2534	2500
$\dot{Q}_{evap}$ (W)	2330	2223	2126	2059	2015	1980
$\dot{Q}_{IHX}$ (W)	94	88	84	82	84	87
$\dot{W}_{comp}$ (W)	493	495	496	502	515	520
COP_{system}	1.30	1.24	1.18	1.14	1.11	1.08

The figure 16 plots a graph of the operating pressure of the condenser against different environment temperatures. It shows that when the temperature increase, the operation pressure increase. The figure also shows that the condenser pressure for R1234yf is about 5% to 10% higher than the condenser pressure for R134a. However, for the R1234yf with IHX, it shows that the system can achieve about 14% to 17% of pressure reduction.

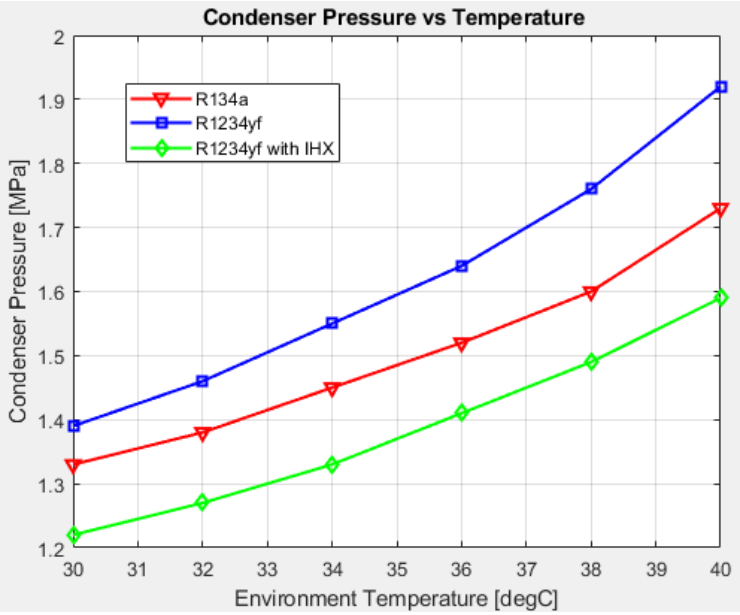

Fig. 16 Condenser Pressure vs Temperature.

The figure 17 below shows the work that was required for the compressor to compress the refrigerants at different environment temperatures. It shows that the average required work for R134a is about 500 to 535W. For the R1234yf, the average required work for is about 6% than the R134a. However, compared to the VCC with IHX, the figure also shows that the average required work is about 8% lower than using R1234yf in VCC without IHX and about 2% lower than using R134a in the same cycle without IHX.

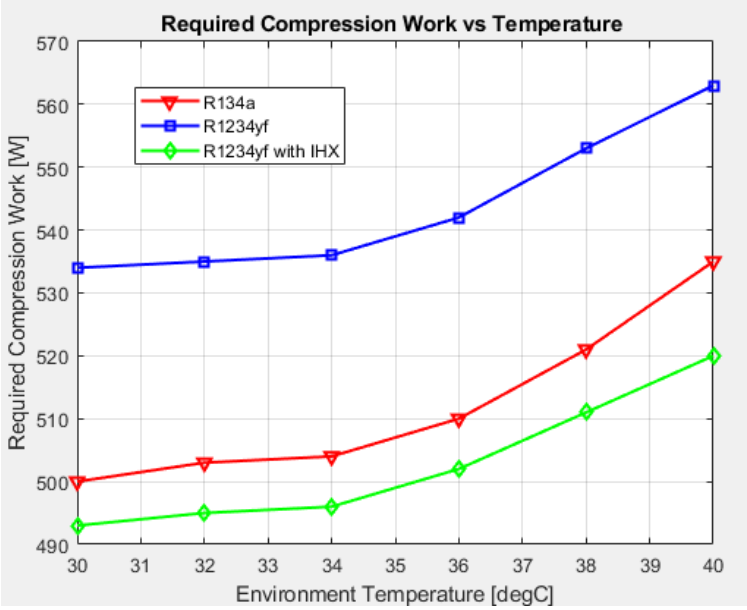

Fig. 17 Required compression Work vs Environment Temperature.

The figure 18 below shows that the actual coefficient of performance which the input power for the Fan and Blower were also considered. When the system is in cooling mode, it shows that the COP_{sytem} using R1234yf is 1.3 and it decreases up to 1.04 at 40 °C. The average COP_{sytem} using R1234yf is about 1 to 3% lower than R134a. However, when the IHX is applied, the COP_{sytem} value for R1234yf is increased slowly as the environment temperature increases and it reaches 1.07 at 40 °C.

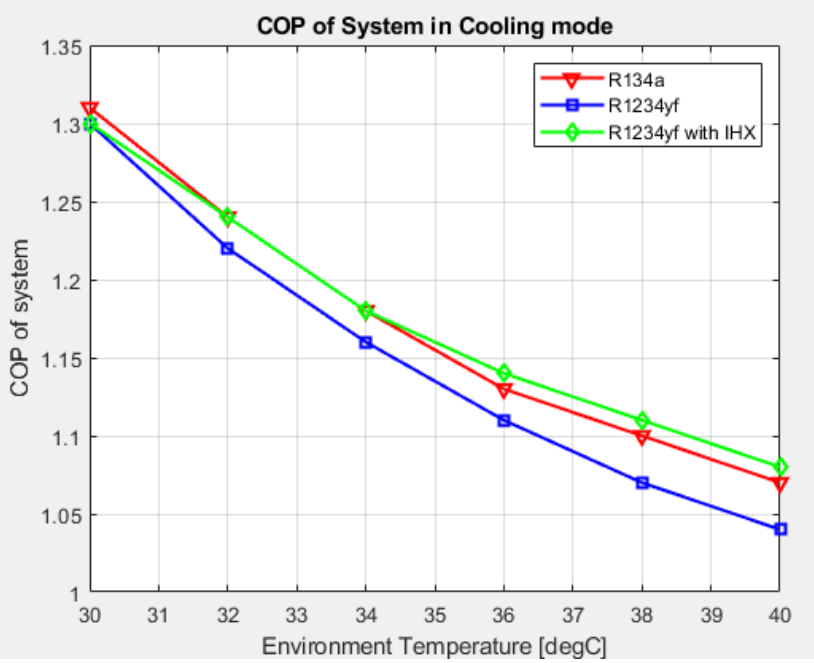

Fig. 18 COP of the system in Cooling mode.

3.11. Results (Heating mode models)

For the heating mode simulation, the Table 10 shows the simulation value from the heating mode model with both refrigerants. In addition, the Table 11 shows the results from the heating mode model with IHX and R1234yf selected as the refrigerants.

Table 10 The simulation results from Heating mode model with R134a and R1234yf

Refrigerant R134a						
Environment Temp (°C)	**-4**	**-2**	**0**	**2**	**4**	**6**
h_1 (kJ/kg)	396	398	399	400	401	402
h_2 (kJ/kg)	432	432	433	434	434	434
h_3 (kJ/kg)	232	232	232	232	233	235
h_4 (kJ/kg]	232	232	232	232	233	235
P_{cond} (Mpa)	1.16	1.22	1.29	1.35	1.37	1.42
P_{evap} (Mpa)	0.21	0.23	0.24	0.26	0.28	0.29
$\dot{Q}_{cond}$ (W)	1948	2263	2603	2960	3336	3720
$\dot{Q}_{evap}$ (W)	1603	1870	2158	2463	2791	3121
$\dot{W}_{comp}$ (W)	344	393	448	504	557	617
COP_{system}	1.18	1.33	1.48	1.64	1.79	1.94
Refrigerant R1234yf						
Environment Temp (°C)	**-4**	**-2**	**0**	**2**	**4**	**6**
h_1 (kJ/kg)	361	362	364	364	365	369
h_2 (kJ/kg)	389	390	391	392	393	394
h_3 (kJ/kg)	232	232	232	232	235	239
h_4 (kJ/kg]	232	232	232	232	235	239
P_{cond} (Mpa)	1.16	1.22	1.28	1.34	1.42	1.52
P_{evap} (Mpa)	0.24	0.25	0.27	0.28	0.30	0.32
$\dot{Q}_{cond}$ (W)	2059	2358	2675	3011	3341	3665
$\dot{Q}_{evap}$ (W)	1688	1942	2210	2496	2763	3012
$\dot{W}_{comp}$ (W)	371	417	468	521	582	651
COP_{system}	1.23	1.37	1.51	1.65	1.78	1.87

Table 11 The simulation results from Heating mode model with IHX using R1234yf

Refrigerant R1234yf with IHX						
Environment Temp (°C)	**-4**	**-2**	**0**	**2**	**4**	**6**
h_1 (kJ/kg)	361	362	363	364	365	366
$h_{1"}$ (kJ/kg)	365	365	368	369	367	368
h_2 (kJ/kg)	393	393	393	393	393	394
h_3 (kJ/kg)	232	232	233	234	235	239
$h_{3"}$ (kJ/kg)	228	228	227	227	228	231
h_4 (kJ/kg]	228	228	227	227	228	231
P_{cond} (Mpa)	1.08	1.12	1.17	1.21	1.25	1.32
P_{evap} (Mpa)	0.23	0.25	0.27	0.28	0.31	0.32
$\dot{Q}_{cond}$ (W)	2042	2323	2615	2920	3256	3575
$\dot{Q}_{evap}$ (W)	1689	1953	2237	2549	2856	3141
$\dot{Q}_{IHX}$ (W)	48	49	47	42	41	39
$\dot{W}_{comp}$ (W)	354	397	442	488	538	599
COP_{system}	1.23	1.37	1.50	1.63	1.77	1.88

The figure 19 shows the condenser pressure at different temperature. The trend shows that when the environment temperature decreases, the condenser pressure decreases for both refrigerant. The figure 19 also shows that when the temperature surpasses 2 °C, the condenser pressure difference between the R134a and R1234yf are getting smaller. Furthermore, the condenser pressure of the R134a and R1234yf in a heat pump cycle were nearly the identical when the temperature drops from 2 °C to -4 °C. On the other hand, the condenser pressure for R1234yf with IHX is about 10 to 13% lower compared to both refrigerant in the system without an IHX.

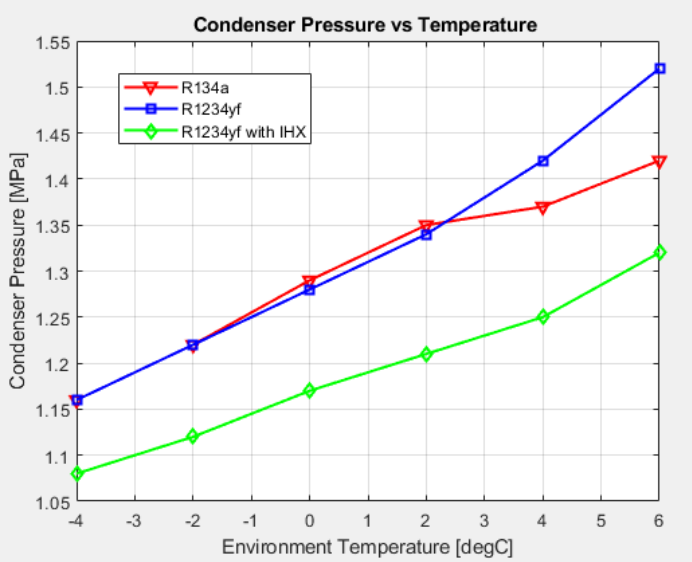

Fig. 19 Condenser Pressure vs Temperature.

The figure 20 below shows the required work for the compressor in the heating mode at different environment temperature. As it is shown in the figure, when the temperature decreases from 6°C to 2°C, the required work decreases for both refrigerants where the value for R1234yf with IHX is about 8% less when compared to R1234yf without IHX, and 3% less than R134a without IHX. However, when the temperature surpasses 0 °C, it is seen that required work for R134a becomes lower than R1234yf with IHX.

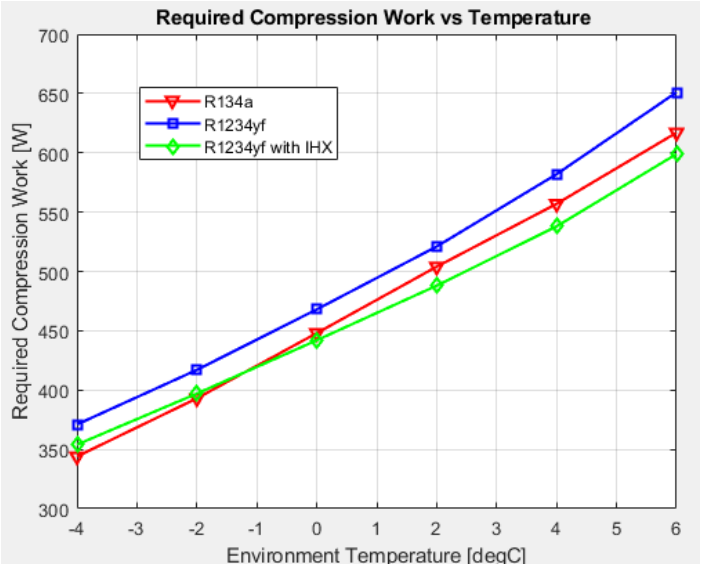

Fig. 20 Required Work for compression vs Temperature.

The figure 21 below shows the actual COP_{sytem} of the system in heating mode with both refrigerants. As it can be seen that the COP_{sytem} of R1234yf and R1234yf with IHX has almost the same value from -4 to 6 degrees Celsius. In addition, the COP_{sytem} of R134a being about 4% lower than both R1234yf and R1234yf with IHX. However, when the temperature surpasses 2°C, the COP_{sytem} of R134a becomes higher compared to the R1234yf and R1234yf with IHX.

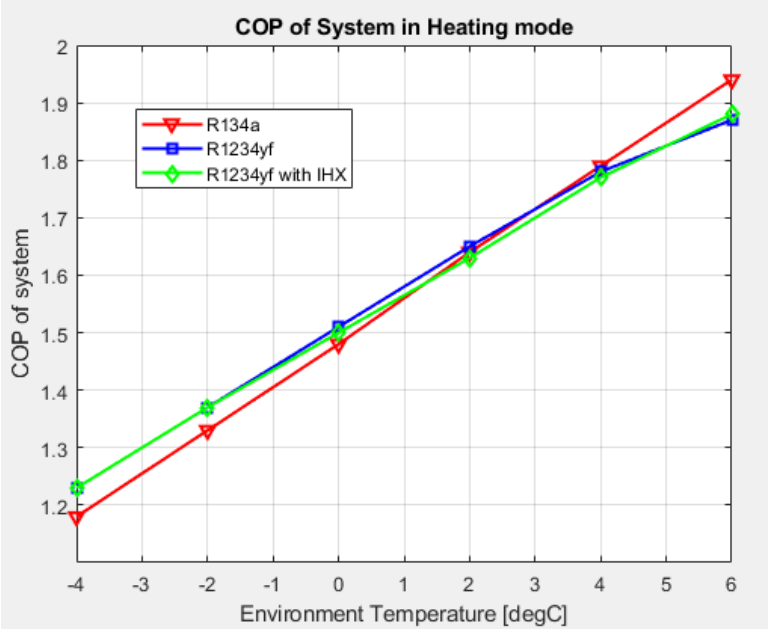

Fig. 21 COP of the system in Heating mode.

4. Conclusion and Further work

In this project, the performance of the HVAC system using alternative refrigerant R1234yf with integrated internal heat exchange had been evaluated. The results show that the R1234yf overall cooling performance is about 3% lower than the refrigerant R134a which was expected due to the difference in thermal properties. Nevertheless, the results also present that the IHX has an effect on the system in terms of performance improvement when the environment temperature increases. It is because the enthalpy difference between the inlet and outlet of the compressor decreases by further superheating from the IHX, as a result, it compensates for the mass flow rate loss due to the increase of refrigerant specific volume.

For the results from the heating mode model, It shows that the pressure at the condenser between the R1234yf and R134a became almost identical when the environment reach 2°C and the COP of the system in heating mode using R134a drops and become lower than R1234yf and R1234yf with IHX, which is a similar result compared to the research that had done by Yıldız, A. & Yıldırım, R[24]

To conclude this, the main goal of this project has been achieved. However, further investigation on IHX effectiveness can be done to maximize the benefit from subcooling the refrigerants and superheating the vapour before compression. Moreover, it is also important to investigate the effect of pressure loss in the IHX as it can increase the power consumption of the compressor.

References

[1] Daanen, H., van de Vliert, E. and Huang, X., 2003. Driving performance in cold, warm, and thermoneutral environments. *Applied Ergonomics*, 34(6), pp.597-602.

[2] Park, M. and Kim, S., 2019. Heating Performance Enhancement of High Capacity PTC Heater with Modified Louver Fin for Electric Vehicles. *Energies*, 12(15), p.2900.

[3] Lee, J., Kwon, S., Lim, Y., Chon, M. and Kim, D., 2013. Effect of Air-Conditioning on Driving Range of Electric Vehicle for Various Driving Modes. *SAE Technical Paper Series*,.

[4] R, F. and J, R., 2000. Impact of Vehicle Air-Conditioning on Fuel Economy, Tailpipe Emissions, and Electric Vehicle Range. US Department of Energy (US).

[5] Jandgassociates.co.uk. 2021. R22 Phase Out Time. [online] Available at: <http://www.jandgassociates.co.uk/Downloads/R22PhaseOut.pdf> [Accessed 14 January 2021].

[6] Reasor, P., Aute, V., and Radermacher, R., "Refrigerant R1234yf Performance Comparison Investigation", *Purdue e-Pubs* Available: http://docs.lib.purdue.edu/iracc/1085.

[7] 3BEAUBIEN, S., LOMBARDI, S., CIOTOLI, G., ANNUZIATELLIS, A., HATZIYANNIS, G., METAXAS, A., and PEARCE, J., "Potential hazards of CO2 leakage in storage systems—Learning from natural systems", *Greenhouse Gas Control Technologies 7*, 2005, pp. 551-560.

[8] Abas, N., Kalair, A., Khan, N., Haider, A., Saleem, Z., and Saleem, M., "Natural and synthetic refrigerants, global warming: A review", *Renewable and Sustainable Energy Reviews*, Vol. 90, 2018, pp. 557-569.

[9]Didion, D., and Brown, J., "Challenges in Developing Environmentally Safe Heat Pumping Systems", *NIST* Available: https://www.nist.gov/publications/challenges-developing-environmentally-safe-heat-pumping-systems.

[10]Park, S., Ahn, J., and Kim, T., "Off-design operating characteristics of an open-cycle air refrigeration system", *International Journal of Refrigeration*, Vol. 35, No. 8, 2012, pp. 2311-2320.

[11]Navarro-Esbrí, J., Mendoza-Miranda, J., Mota-Babiloni, A., Barragán-Cervera, A., and Belman-Flores, J., "Experimental analysis of R1234yf as a drop-in replacement for R134a in a vapor compression system", *International Journal of Refrigeration*, Vol. 36, No. 3, 2013, pp. 870-880.

[12]Pottker, G., and Hrnjak, P., "Effect of the condenser subcooling on the performance of vapor compression systems", *International Journal of Refrigeration*, Vol. 50, 2015, pp. 156-164.

[13]"Suction line heat exchangers - Heat Exchanger Design Handbook, Multimedia Edition", *Hedhme.com* Available: https://hedhme.com/content_map/?link_id=360&article_id=402.

[14]Miller, R., and Miller, M., *Air conditioning and refrigeration*, New York, N.Y.: McGraw-Hill Professional, 2012.

[15]J. H, D., and R. R, C., "Modeling of an Automotive Air Conditioning Compressor Based on Experimental Data", *Ideals.illinois.edu* Available: https://www.ideals.illinois.edu/bitstream/handle/2142/9703/TR014.pdf?sequence=2&isAllowed=y.

[16]Mota-Babiloni, A., Navarro-Esbrí, J., Barragán, Á., Molés, F., and Peris, B., "Drop-in energy performance evaluation of R1234yf and R1234ze(E) in a vapor compression system as R134a replacements", *Applied Thermal Engineering*, Vol. 71, No. 1, 2014, pp. 259-265.

[17]"Engineering:Corrected flow - HandWiki", *Handwiki.org* Available: https://handwiki.org/wiki/Engineering:Corrected_flow.

[18]Shah, R., and Dušan, P., *Fundamentals of Heat Exchanger Design*, John Wiley & Sons, 2003.

[19]Incropera, F., and DeWitt, D., *Fundamentals of Heat and Mass Transfer*, 2000.

[20]Eames, I., Milazzo, A., and Maidment, G., "Modelling thermostatic expansion valves", *International Journal of Refrigeration*, Vol. 38, 2014, pp. 189-197.

[21]Çengel, Y., *Heat transfer*, Boston (Mass.): McGraw-Hill, 2006.

[22]SM J, J., S, S., K, K., and G, N., "Design of ROVAC Air-Conditioning System for a Car", 2016.

[23]Moran, M., and Shapiro, H., *Fundamentals of engineering thermodynamics*, Hoboken: Wiley, 2014.

[24]Yıldız, A., and Yıldırım, R., "Investigation of using R134a, R1234yf and R513A as refrigerant in a heat pump", *International Journal of Environmental Science and Technology*, Vol. 18, No. 5, 2020, pp. 1201-1210.